

Simulation of Integrin-Cytoskeletal Interactions in Migrating Fibroblasts

Christine E. Schmidt, Tani Chen, and Douglas A. Lauffenburger[†]

Department of Chemical Engineering and [†]Biophysics Program, University of Illinois, Urbana, Illinois 61801 USA

ABSTRACT Cell migration is a dynamic phenomenon requiring a physical interaction between the internal cell motile machinery and the external substratum in which adhesion receptors, such as integrins, serve as the transmembrane link. To analyze quantitatively this interaction, we apply a modified Brownian dynamics algorithm to simulate cytoskeleton-mediated transport of integrin on the dorsal surfaces of migrating fibroblasts. Previously, we experimentally demonstrated that integrin is transported in an intermittent fashion, with directed excursions interspersed by diffusive periods, preferentially toward the cell edge where the integrin is likely used in the formation of nascent adhesions. Integrins containing mutations in the cytoskeleton-binding region of the cytoplasmic domain display statistically different degrees of directed transport, indicating that this phenomenon is dependent on cytoskeletal associations. In the present work, we develop a computer algorithm generating simulated integrin transport trajectories, given estimates for the rate constants defining coupling (k_c) and uncoupling (k_u) of integrin with cytoskeletal components. Other parameters supplied to the program, the diffusion coefficient (D) for integrin in the membrane and the instantaneous velocity (v_i) of the integrin/cytoskeleton complex, have been measured independently in our experimental system. By comparing the simulated trajectories with those obtained experimentally, we are able to estimate the coupling and uncoupling rate constants for the interaction of integrin with cytoskeletal elements *in vivo*. We find that integrin couples with cytoskeletal elements at a rate approximately 10 times slower than its rate of uncoupling ($k_c = 0.3 \text{ s}^{-1}$, $k_u = 3 \text{ s}^{-1}$). Comparison of these rate constants with an equivalent rate constant for diffusion, $k_d = 0.4 \text{ s}^{-1}$, indicates that the coupling interaction is likely a diffusion-limited process, as is typically expected for membrane processes. We further show by calculation that directed transport is necessary for integrin to traverse the length of an extending lamellipod to its leading edge; diffusion alone is not sufficiently fast to supply adhesion receptors to points of new cell/substratum contact.

INTRODUCTION

Cell locomotion is fundamental to numerous biological processes in the vertebrate body including wound healing, inflammation, cancer metastasis, angiogenesis, embryonic development (Trinkaus, 1984), and the colonization of bio-artificial organs and tissues (Cima et al., 1991). A critical factor for cell migration is the adhesive interaction of the cell with its substratum. Contacts are typically mediated by transmembrane adhesion receptors, such as the integrins, that link the internal cytoskeleton and its associated motors to extracellular surfaces (Horwitz et al., 1986; Burridge et al., 1988; Otey et al., 1990). This linkage in turn allows contractile forces within the cell to be transmitted as traction forces along a nondeformable surface (Singer and Kupfer, 1986; Heidemann et al., 1990; Wang et al., 1993). Although these contacts are critical for the locomotory process, little is known concerning the regulation of the formation and release of these transmembrane linkages within the moving cell (Regen and Horwitz, 1992). Furthermore, the process by

which integrins are supplied to areas where these contacts develop is poorly understood. The focus of this paper is to understand better the means by which integrins are supplied to the cell's leading edge where nascent adhesions are formed.

We have previously used video microscopy and image analysis techniques to demonstrate that 40-nm beads coated with anti- $\beta 1$ integrin monoclonal antibodies (mAbs) are rapidly and intermittently transported forward on migrating mouse fibroblasts (Schmidt et al., 1993). The observed rapid, directed motions are statistically distinct from diffusion because they give rise to overall displacements that cannot be accounted for by pure diffusion. These transport events, consisting of rapid excursions interspersed with diffusion, are of interest because they could play a mechanistic role in cell migration by providing integrins to the cell's advancing edge where nascent adhesions are formed. Importantly, we employed cells transfected with $\beta 1$ integrins mutated by various degrees in the cytoplasmic domain to demonstrate that directed transport of integrin appears to require specific biochemical information in the $\beta 1$ cytoplasmic domain. In the first place, a mutant integrin lacking its entire cytoplasmic domain essentially underwent pure diffusion, suggesting that the normal directed transport process involves the interaction of integrin with a cytoskeletal component that gives rise to brief, rapid excursions. Furthermore, mutant integrins containing particular single amino acid substitutions in the cytoplasmic domain did not exhibit significant directed excursions—similarly to the truncation mutant, indicating that directed transport involves a cytoskeletal-coupling event

Received for publication 10 February 1994 and in final form 13 April 1994.

Address reprint requests to Douglas A. Lauffenburger, Department of Chemical Engineering, 114 Roger Adams Laboratory, Univ. of Illinois-Urbana-Champaign, 600 South Mathews Ave., Urbana, IL 61801. Tel.: 217-333-9141; Fax: 217-244-8068; E-mail: lauffen@aries.scs.uiuc.edu.

A copy of the simulation program is available (in uncompiled form) upon request. Please address any inquiries to the corresponding author.

Abbreviations used: $\beta 1$, chicken $\beta 1$ integrin; MSD, mean-square displacement; mAb, monoclonal antibody; WT, wild-type.

© 1994 by the Biophysical Society

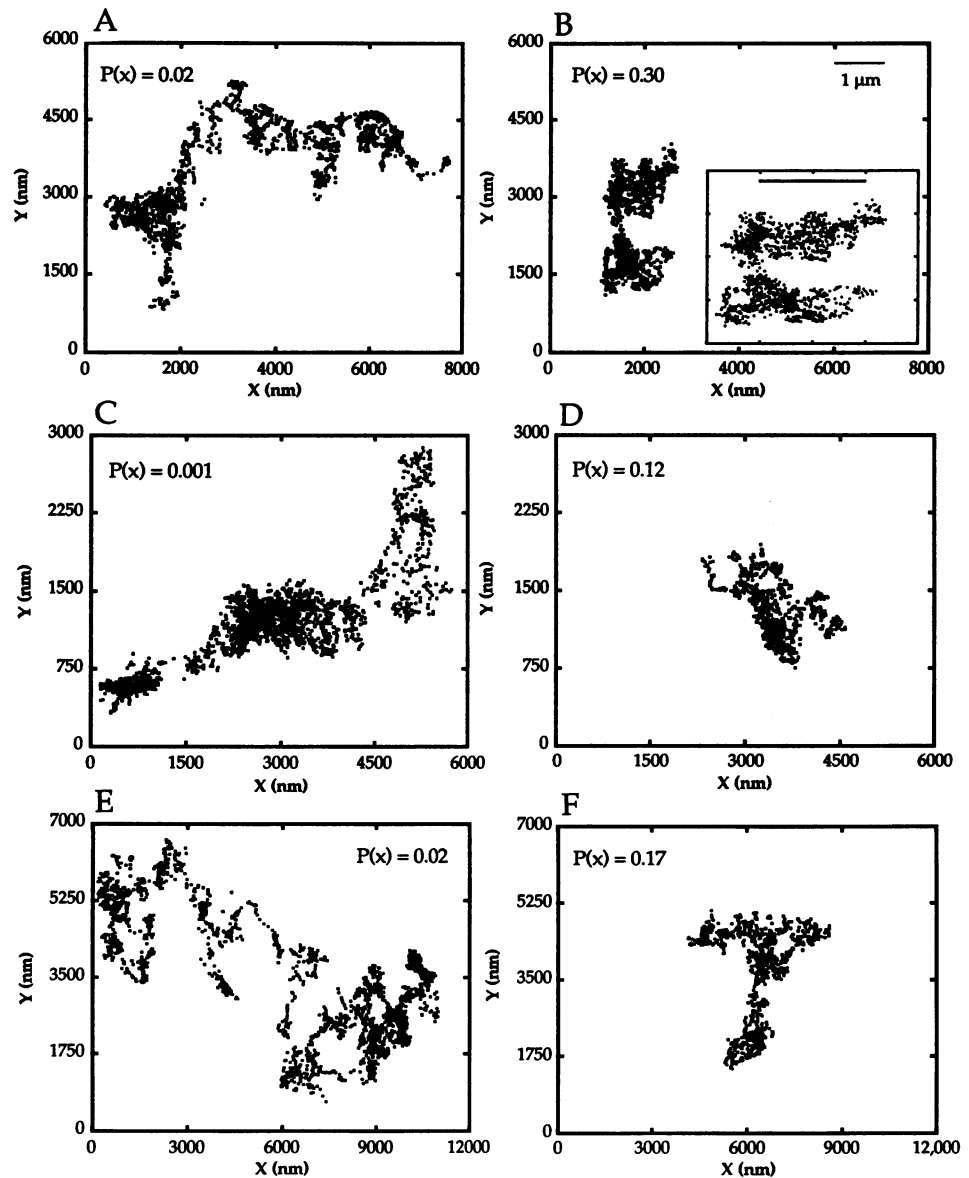
0006-3495/94/07/461/14 \$2.00

and that the lack of interaction between mutated integrin and the cytoskeleton is likely not the result of merely a nonspecific steric interaction.

In our current work, we develop a computer algorithm to simulate the diffusive as well as directed nature of integrin transport. Integrin movement is modeled as a two-dimensional random walk with an added probability for linkage to a moving cytoskeletal element. The probabilities for coupling to and uncoupling from the cytoskeletal element during a particular time interval are proportional to the coupling and uncoupling rate constants, respectively, for integrin-cytoskeleton associations. By supplying experimentally determined values for the diffusion coefficient, the instantaneous velocity for the moving integrin-cytoskeleton complex, and the obtained best-fit values for the coupling and uncoupling rate constants for integrin-cytoskeleton coupling, we can successfully simulate paths for integrin transport.

Using an iterative scheme to minimize the deviation between experimental and simulated results, we find that integrin interacts reversibly with the moving cytoskeletal element at rates characterized by the coupling and uncoupling rate constants, $k_c = 0.26 \pm 0.025 \text{ s}^{-1}$ and $k_u = 2.5 \pm 0.24 \text{ s}^{-1}$, respectively. The values for k_c and k_u are effective values that reflect intrinsic reaction rates and a diffusion effect. Calculation of an equivalent rate constant for diffusion indicates that the overall coupling interaction is a diffusion-limited process that is typical for most membrane processes. We also demonstrate mathematically that diffusion alone is not sufficient to provide most integrins to the cell's leading edge but that directed transport can account for this delivery. Therefore, we have used computer simulations to estimate in vivo coupling and uncoupling rate constants for integrin's association with the moving cytoskeletal element that gives rise to directed transport. Knowledge of the time-scales for these interactions could potentially be incorporated into mecha-

FIGURE 1 Experimental trajectories for integrin undergoing either directed transport or pure diffusion. In a previous study, we coated 40 nm colloidal gold particles with anti-integrin monoclonal antibodies, then used video microscopy and image analysis techniques to track individual gold particles on the surfaces of migrating cells (Schmidt et al., 1993). Panels A, C, and E are paths, each classified as directed ($P(x) < 0.05$), for three different gold particles bound to WT integrin. Panels B, D, and F are trajectories, all scored as diffusive ($P(x) \geq 0.05$) for beads bound to integrin truncated in its cytoskeleton-binding domain, 765t. The inset, an enlargement of the path shown in panel B, illustrates the detailed character of the diffusive trajectory. The scale bars in both panel B and the inset are $1 \mu\text{m}$. Adjacent plots ((A, B), (C, D), (E, F)) have the same scales for the x and y axes.



nistic models describing integrin-based adhesion or locomotion processes for cells.

MATERIALS AND METHODS

Experimental background

In our previous study (Schmidt et al., 1993), we monitored colloidal gold particles coated with anti-integrin mAbs to demonstrate that $\beta 1$ integrin is transported to the leading edge of migrating cells by a cytoskeleton-dependent event. The gold particles bound to the integrins were tracked at video rate, 30 frames/s, over 100 s using an image processor and the cross-correlation method of Gelles et al. (1988). Directed transport was assessed for each integrin path by comparing the net displacement of the integrin with that predicted by pure diffusion. If the probability $P(x)$ that diffusion could give rise to the measured displacement (x) was less than 0.05, then the integrin path was scored as directed. For $P(x) \geq 0.05$, the integrin path was considered diffusive. The percent directed character was calculated as the percentage of total tracked integrins undergoing directed transport.

The system that we used for these studies consisted of mouse fibroblasts that were transfected with chicken $\beta 1$ ($\beta 1_c$) integrins mutated by various degrees in the cytoskeleton-binding region of the cytoplasmic domain. WT integrin is nonmutated $\beta 1_c$ integrin and exhibits a high frequency of directed transport to the front edges of migrating cells ($60 \pm 13\%$ of the tracked gold particles underwent directed transport). In contrast, the 765t integrin, which has a truncated cytoplasmic domain, does not display significant levels of directed transport and, instead, essentially undergoes pure diffusion ($7 \pm 9\%$ of the tracked gold particles were scored as directed). These data indicate that the interaction of the integrin cytoplasmic domain with a moving cytoskeletal element likely gives rise to the directed transport of WT integrin. Fig. 1 illustrates examples of experimentally observed paths for WT integrin undergoing directed transport (Fig. 1 A, C, E) and for the truncated integrin, 765t, diffusing (Fig. 1 B, D, F).

In addition to monitoring the overall directed character of integrin, we also constructed mean-square displacement (MSD) versus time plots for each path from which we could determine the two-dimensional diffusion coefficient and the time-averaged velocity for directed motions. Diffusivities for the WT and truncated integrins were determined from two-dimensional MSD versus time plots as previously described (Schmidt et al., 1993). For WT integrin, $D = (3.6 \pm 3.3) \times 10^{-10} \text{ cm}^2/\text{s}$ and for the truncated integrin, $D = (3.4 \pm 2.3) \times 10^{-10} \text{ cm}^2/\text{s}$, with an average for the WT and 765t integrins of $D = (3.5 \pm 2.8) \times 10^{-10} \text{ cm}^2/\text{s}$. The time-averaged velocity for directed transport was calculated for the WT integrin as $\langle v \rangle = 4.5 \pm 4.5 \mu\text{m}/\text{min}$. This value was estimated from one-dimensional MSD versus time plots ($MSD = 2Dt + \langle v \rangle^2 t^2$) for only those gold particles undergoing directed transport.

The time-averaged velocity, $\langle v \rangle$, represents the average velocity of the moving integrin assuming a constant external force over the entire path observed. However, from our experiments, we found that the integrin undergoes brief intervals of directed motion interspersed with periods of pure diffusion. In addition, there were portions of the integrin trajectories that appeared to involve a combination of directed excursions and diffusion, likely a rapid association/dissociation from a moving cytoskeletal element. Because the time-averaged velocity is an average velocity for the entire path, it is not an adequate measure of the intrinsic, instantaneous velocity of the moving cytoskeletal element or of the instantaneous velocity of the moving integrin/cytoskeleton complex. We determined an average value for the instantaneous velocity, v_i , of the moving integrin/cytoskeleton complex from 30 segments of experimental integrin trajectories that were undergoing obvious rapid excursions. These excursions could not be accounted for by pure diffusion using the same statistical methods as mentioned above. Directed intervals occurring over a period of 1–2 s were used to minimize potential noise from the experimental tracking routine. The displacements and time intervals for the excursions were used to calculate the instantaneous velocity as $v_i = 37 \pm 15 \mu\text{m}/\text{min}$.

Does the behavior of each gold particle represent a single-integrin binding event? We used varying concentrations of antibody on the colloidal gold particles and also monitored various gold bead sizes (40 to ~ 100

nm) to find no differences in directed transport events (our unpublished observations). These results suggest that various degrees of aggregation for integrins (and single integrins, if we “extrapolate” to a single antibody per contact site on the gold particles) do not affect the directed transport of this molecule.

Simulations: overview

We have developed a computer algorithm, using a Brownian dynamics approach (McCammon, 1991), to simulate the diffusive as well as directed nature of integrin transport to the cell’s leading edge. Fig. 2 illustrates the major elements of our stochastic model.

The program conducts a nonbiased two-dimensional random walk with a probability for linkage to a moving cytoskeletal element. The probability of linkage (P_c) is the product of the time step (Δt) and the estimated rate constant for coupling (k_c) (see Appendix A). The time step used in the simulation was 1/30 s, which is equivalent to the time scale used in the gold particle tracking experiments. If the probability for linkage, P_c , is high, then integrin is more likely to link to the cytoskeletal element during a particular time step. When linked, integrin is displaced a distance proportional to the product of the velocity of the moving cytoskeletal element (v_i) and Δt . The cytoskeletal element is assumed to be moving unidirectionally in the $+x$

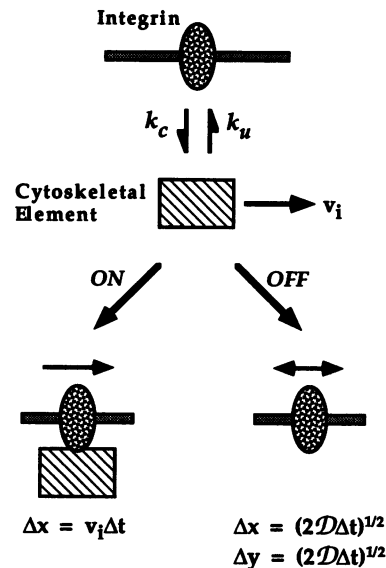


FIGURE 2 Schematic representation of the major assumptions for dynamic coupling model. To simulate the directed and diffusive nature of integrin transport, we have modeled integrin’s behavior in the cell surface as a two-dimensional random walk with an added probability for linkage to a moving cytoskeletal element. Integrin’s interaction with the cytoskeletal element is characterized by the coupling and uncoupling rate constants, k_c and k_u respectively. The cytoskeletal element is assumed to be moving unidirectionally in the $+x$ direction at a velocity v_i , which is consistent with our experimental observation that directed motions occur predominantly in one direction. During a particular time interval ($\Delta t = 1/30 \text{ s}$) if integrin links to the cytoskeletal element, then it will displace in the $+x$ direction proportional to the velocity of the moving cytoskeletal unit, $\Delta x = v_i \Delta t$. If integrin does not interact with the cytoskeleton in a given time step, then it will be free to diffuse in the membrane and its displacement will be proportional to integrin’s diffusivity, $\Delta x = (2D\Delta t)^{1/2}$ and $\Delta y = (2D\Delta t)^{1/2}$. Both D and v_i have been experimentally determined from the gold particle trajectories as described in Materials and Methods ($D = 3.5 \times 10^{-10} \text{ cm}^2/\text{s}$ and $v_i = 37 \mu\text{m}/\text{min}$). Therefore, the only unknowns in our model are the values for k_c and k_u , which will be determined by iteratively matching the character of the simulated trajectories to those for the experimental paths (refer to Figs. 4 and 5).

direction, which is consistent with our experimental observation that directed motions occur predominantly in one direction. In addition, the instantaneous velocity of the moving cytoskeletal element is assumed to be constant for a given cell type and independent of integrin's ability to interact with the element. We found from the gold particle tracking experiments that the instantaneous velocity did not vary significantly for different integrin mutants, validating our assumption.

If integrin becomes attached to the cytoskeleton in the first time step, then during the next time interval it can either remain attached or it can dissociate with a probability (P_u) equal to the product of the uncoupling rate constant (k_u) and Δt . If uncoupled from the cytoskeleton, integrin displaces a distance proportional to $(2D\Delta t)^{1/2}$ in both the x and y directions, where D is the diffusivity input to the program. This process is repeated at each time step for a total time of 100 s which, as previously mentioned, is the total analysis time used for the gold particle tracking experiments.

Estimates for k_c and k_u , in addition to the supplied experimental values for D and v_i , can be used to simulate the diffusive and directed transport character of integrin. Once simulated, each trajectory is statistically analyzed using the same methodology as applied to the experimental paths. Values for k_c and k_u are supplied iteratively to the program until the character of the simulated paths matches those obtained experimentally. Ultimately, values for k_c and k_u , which reflect the dynamics of directed transport, can be determined for integrin.

Initial estimates for k_c and k_u were determined based on values for K_D (k_u/k_c) estimated from our previous colloidal gold tracking experiments. The fraction of integrin's path that is directed can be written as a ratio of the directed displacement to the total displacement, based on the probabilities for coupling and uncoupling from a cytoskeletal element in a single time step:

$$\text{Fraction of Path Directed} = \frac{(k_c \Delta t) v_i \Delta t}{(k_u \Delta t)(2D\Delta t)^{1/2} + (k_c \Delta t) v_i \Delta t} \quad (1a)$$

$$= \frac{1}{1 + (k_u/k_c) \frac{(2D\Delta t)^{1/2}}{v_i \Delta t}} \quad (1b)$$

Thus,

$$K_D = (k_u/k_c) = \frac{v_i \Delta t}{(2D\Delta t)^{1/2}} [(1/\text{Fract.Dir.}) - 1] \quad (1c)$$

The directed fraction for each path was assessed for integrin based on the average velocity for integrin's path, extracted from the *MSD* versus time plot, and the instantaneous velocity for a directed jump, v_i . Note that the directed fraction for each path is not identical to the percent directed character mentioned previously, which was the fraction of cells exhibiting a significantly directed path. The average fraction directed, a value of 1/30 s for Δt , and the average values for v_i (37 $\mu\text{m}/\text{min}$) and D ($3.5 \times 10^{-10} \text{ cm}^2/\text{s}$) were used to evaluate Eq. 1c, yielding an initial estimate of $K_D = 4.3 \pm 4.5$ for integrin.

Simulations: algorithm

The simulation program was written in FORTRAN and was run either on an IRIS Indigo Workstation (Silicon Graphics) or on a VAX mainframe computer. Validation of consistency between the two systems was accomplished by comparing the results from multiple runs on each machine. A schematic of the program algorithm is shown in Fig. 3.

First, estimates for k_c and k_u are chosen and $D = 3.5 \times 10^{-10} \text{ cm}^2/\text{s}$ and $v_i = 37 \mu\text{m}/\text{min}$ are supplied to the program. Initially, integrin is not linked to any cytoskeletal components. For each time step of $\Delta t = 1/30$ s, a random number, R , is generated from a uniform distribution between 0 and 1 (see below). R is compared to the probability that integrin can either link to a cytoskeletal element, $P_c = k_c \Delta t$, or detach from a cytoskeletal element, $P_u = k_u \Delta t$, depending on the current unbound or bound state, respectively, of integrin (see Appendix A). If $R < P$, then integrin changes its state of linkage during that time interval.

Linked integrin is transported a distance $\Delta x = v_i \Delta t$ and $\Delta y = 0$. Unlinked integrin diffuses a distance $\Delta x = (2D\Delta t)^{1/2} w_x$ and $\Delta y = (2D\Delta t)^{1/2} w_y$, where

w_x and w_y are random numbers generated from a $N(0, 1)$ distribution (i.e., a Normal distribution with mean zero and SD = 1). The variables w_x and w_y reflect the stochastic nature of diffusion and account for the random direction and magnitude of a diffusive step.

This process of comparing generated random numbers (R) to the probability for linkage or unlinkage to the cytoskeletal element during a given time interval, is repeated for each time step for a total of 100 s. The simulated path is then classified as either diffusive or directed using statistical techniques as described below. A minimum of 400 paths are generated for each k_c/k_u pair, and the percentage of paths scored as undergoing directed transport (*%Dir*) is calculated and compared to the experimental value for integrin (60%). In addition, the time-averaged velocity for directed transport, $\langle v \rangle = 4.5 \mu\text{m}/\text{min}$ as determined from experimental parallel MSD versus time data, is also compared with the value calculated from the simulated trajectories. If the simulated and experimental *%Dir* and $\langle v \rangle$ do not match, then new estimates for k_c and k_u are entered and the entire process is repeated. This iterative process results in values for k_c and k_u that reflect the dynamics of the transient integrin/cytoskeleton interactions that give rise to intermittent, directed transport.

Note that both the coupling and uncoupling rate constants have units of s^{-1} so that the probabilities for linkage and unlinkage, $P_c = k_c \Delta t$ and $P_u = k_u \Delta t$; are dimensionless. In other words, the coupling rate constant includes an effective local concentration of the cytoskeletal component with which integrin interacts, $k_c [\text{s}^{-1}] = k_c (\text{intrinsic}) [\text{M}^{-1} \text{s}^{-1}] * [\text{cytoskeletal component}] [\text{M}]$. The uncoupling rate constant, k_u , does not depend on the concentration of the cytoskeletal component and has intrinsic units of s^{-1} .

The simulation program was tested by generating thousands of diffusive paths with a given diffusion coefficient, D , and $k_c, k_u = 0$. Simulated paths were subjected to the analysis described below to generate D . The mean value for D was the same as that input to the program. In addition, the average displacement of the paths was equal to that predicted statistically from D (see below, Analysis of Trajectories).

Random number generators

Random numbers between 0 and 1 (uniform distribution) were generated using the portable RAN1 algorithm consisting of three linear congruential generators with a mixing routine (Press et al., 1986). Seeds for the random number generator were selected from a shuffled list of integers between 0 and -54773. When necessary, random numbers were selected from a Normal (Gaussian) distribution according to the routine GasDev outlined in Press et al. (1986). The GasDev function returns a normally distributed deviate with zero mean and unit variance, using RAN1 as the source of uniform deviates.

Simulations: analysis of trajectories

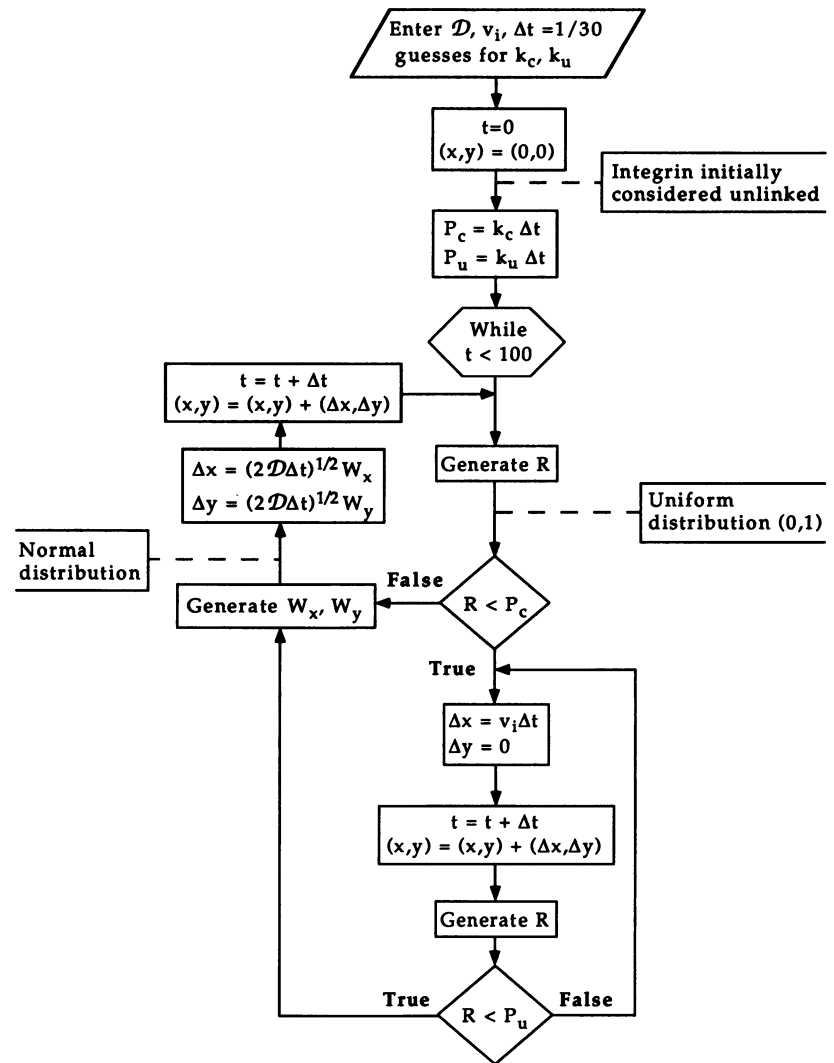
Directed and diffusive motion were differentiated statistically as previously described (Schmidt et al., 1993). The net displacement of each simulated path for the total tracking time of 100 s was determined and compared to the distance predicted if only diffusion produced the displacement. The statistical probability that a particle undergoing a random walk will diffuse to a distance between x and $x + dx$ is described by Berg (1983) in the equation

$$P(x)dx = 1/(4\pi Dt)^{1/2} \exp(-x^2/4Dt)dx \quad (2)$$

where t is the time interval over which x is measured, and D is the two-dimensional diffusivity. Integrating the above equation from x to ∞ yields the probability, $P(x) = \text{erf}(x/\sqrt{4Dt})$, that a particle has diffused a distance greater than the actual displacement, x . Simpson's integration was used to solve Eq. 2 within the simulation. A significance level for $P(x)$ of 0.05 was used. That is, particle displacements with $P(x) \geq 0.05$ were scored as diffusive, and those with $P(x) < 0.05$ were considered directed.

Values for the diffusivity, D , and the time-averaged velocity of directed motion, $\langle v \rangle$, were extracted from MSD versus time data for each simulated path. The diffusion coefficient, D , was determined from two-dimensional data via the equation $MSD = 4Dt + \langle v \rangle^2 t^2$. The time-averaged velocity for directed motion was obtained from a 2nd order polynomial fit of parallel

FIGURE 3 Flow chart depicting the algorithm used for dynamic transport simulations. Experimentally determined D and v_i , as well as estimates for k_c and k_u , are input to the program. The probability for coupling of integrin to the cytoskeleton during a given time step is calculated as $P_c = k_c \Delta t$, and the probability for integrin to uncouple, once it is linked, is $P_u = k_u \Delta t$ (see Appendix A). Integrin is initially not considered linked to the underlying cytoskeletal element. During the initial time step ($\Delta t = 1/30$ s, which is same time-scale used for gold tracking experiments) a random number between (0, 1) is generated from a uniform distribution. This random number is compared to the probability for integrin's coupling to the cytoskeleton, P_c ; if $R < P_c$, then integrin is considered linked during that time interval and it displaces $\Delta x = v_i \Delta t$. If $R > P_c$, then integrin does not successfully couple and it will displace $\Delta x = (2D\Delta t)^{1/2} w_x$ and $\Delta y = (2D\Delta t)^{1/2} w_y$. The variables w_x and w_y are random numbers generated from a Gaussian distribution to account for the stochastic nature of diffusion. This process of generating a random number and comparing it with the probability for coupling or uncoupling, depending on the current unlinked or linked state of integrin, is repeated at each time step for a total time of 100 s. The resulting simulated path is then scored as diffusive or directed as described in Materials and Methods. In addition, the time-averaged velocity, $\langle v \rangle$, for directed transport is calculated from the trajectory data. Hundreds to thousands of paths are generated for each k_c/k_u pair, and the percentage of paths undergoing directed transport ($\%Dir$) and the average $\langle v \rangle$ are determined. New k_c/k_u values can be supplied to the program until the character of the simulated paths, $\%Dir$ and $\langle v \rangle$, matches that of the experimental paths. This matching process is described in Materials and Methods and is outlined in Figs. 4 and 5.



MSD data to the function $MSD = 2Dt + \langle v \rangle^2 t^2$ (Sheetz et al., 1989). After generation of (x, y) coordinates for a simulated path, the data were fit to a straight line using the LINPACK linear least-squares fitting routine (Dongarra et al., 1979). This line defined the major axis for directed transport and subsequently, parallel MSD data were generated for each time point by determining the displacement of the simulated path parallel to this line. A linear parallel MSD versus time relationship is indicative of pure diffusion, $MSD = 2Dt$, and a nonlinear relationship with an upward curvature is characteristic of a particle undergoing both directed motion and diffusion, $MSD = 2Dt + \langle v \rangle^2 t^2$.

Where reported, the SD for a proportion (percentage) was calculated for a binomial proportion distribution as $\sqrt{pq/n}$, where p is the proportion of occurrences in a population, q is the proportion of nonoccurrences ($q = 1 - p$), and n is the number of items in a sample (Croxtton, 1958; Wagner, 1992).

Simulations: matching simulation to experiment

Values for k_c and k_u are manually supplied in an iterative fashion to the simulation program until the character of the simulated paths matches that of the experimental trajectories. Ultimately, this matching process yields values for k_c and k_u that reflect the dynamics of the transient integrin/cytoskeleton interactions that give rise to intermittent, directed transport. To match simulations to experiment, we have defined a deviation parameter, ϵ . This parameter is a numerical representation of the difference between the means of the fitted values, $\%Dir$ and $\langle v \rangle$, obtained from simulations and

experiment (annotated by the subscripts s and e , respectively):

$$\epsilon = \left(\frac{(\%Dir_e - \%Dir_s)}{\%Dir_e} \right)^2 + \left(\frac{(\langle v \rangle_e - \langle v \rangle_s)}{\langle v \rangle_e} \right)^2 \quad (3)$$

Simulations were run for various values of $K_D = k_u/k_c$. For each value of K_D , k_c was bounded between 0 and $30/K_D$, which roughly yields $P_u \approx 0.5$. The deviation parameter was calculated for each set of at least 400 runs for every k_c/k_u pair. Plots of ϵ vs. K_D and ϵ vs. k_c were constructed and used to determine the values for K_D and k_c that minimize the difference between simulation and experiment (cf. Figs. 4 and 5).

The uncertainty in the value for k_c was estimated from the deviation in ϵ for the given K_D that minimizes ϵ . For this value of K_D , a plot of ϵ vs. k_c indicates the sensitivity of the output to k_c . The uncertainty in k_c was determined as the range of values of k_c for which ϵ varies to three times its minimum value.

RESULTS

Determination of K_D , k_c , and k_u for integrin/cytoskeleton interactions

We have written a computer program to simulate the diffusive as well as directed nature of integrin transport to the cell's leading edge. This model assumes that integrin either diffuses in the cell membrane with a known diffusivity or

transiently couples to a cytoskeletal element moving at a known velocity. We demonstrate that our stochastic model can successfully predict integrin trajectories: given experimental values for integrin diffusivity, D , and the instantaneous velocity of the moving cytoskeletal element, v_i , we have been able to match the percent directed character ($\%Dir$) and the time-averaged velocity ($\langle v \rangle$) of directed motion for integrin.

To match the character of simulated trajectories with those obtained experimentally, we have defined a deviation parameter, ϵ (see Eq. 3). Because the deviation parameter is a measure of the "goodness of fit" between simulation and experiment, we express the results of all simulations in terms of ϵ . Our model contains two unknowns, k_c and k_u . Therefore, we have chosen first to determine the conditions that best simulate experiment by finding the value for $K_D = k_u/k_c$ that minimizes ϵ (Fig. 4). Each point for a given value of K_D represents the average of at least 400 simulations for a unique k_c/k_u pair. As illustrated in Fig. 4, there is a single value, $K_D = 9.5$, that minimizes the deviation ($\epsilon_{\min} = 2.5 \times 10^{-5}$) between simulated and experimental trajectories for integrin transport.

The optimum k_c for integrin-cytoskeleton interactions was estimated from a plot of ϵ vs. k_c for the various K_D values (Fig. 5). Each curve in Fig. 5 represents a different value for K_D

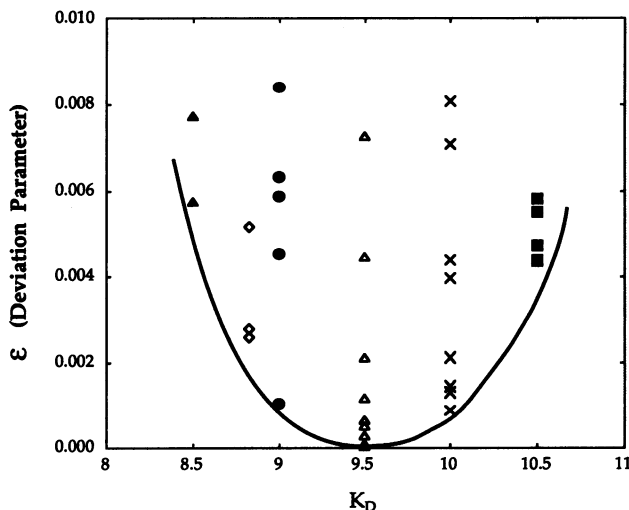


FIGURE 4 Matching simulated and experimental output to obtain a best-fit K_D . To match iteratively the output of the simulations to our experimental data, we have defined a deviation parameter, ϵ . The deviation parameter is a numerical measure of the difference between the means of the fitted values, $\%Dir$ and $\langle v \rangle$, obtained from simulations and experiment. Because our model has two unknowns, k_c and k_u , we chose to determine first the conditions that best simulate our experimental observations by finding the value of K_D that minimizes ϵ . This figure illustrates the calculated deviation parameter for simulations run with various values of K_D . Each data point for a given K_D value represents the average result of a minimum of 400 simulations for a unique k_c/k_u pair; values for k_c were varied over the largest possible range as described in Materials and Methods. As shown, there is a single K_D value (9.5) that minimizes the differences between simulated and experimental trajectories. The parabolic line is not a fit of the data, but rather serves visually to demonstrate the trend for the simulation output. In addition, values of ϵ for smaller and larger values of K_D have been calculated from simulations and are consistent with the trend shown in the figure.

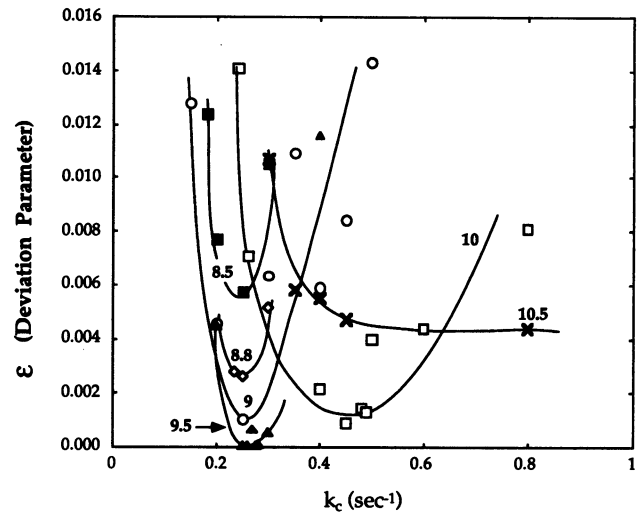


FIGURE 5 Matching simulated and experimental output to obtain a best-fit k_c . This figure illustrates the calculated deviation parameter, ϵ , for simulations run with various values of k_c for the same K_D values shown in Fig. 4. Each curve (not a fit, but rather drawn to help visualize data trends) represents a given K_D value, and each data point for a given curve depicts the average result of a minimum of 400 simulations for a unique k_c/k_u pair. The difference between simulated and experimental paths is minimized for $K_D = 9.5$ and $k_c = 0.26 \text{ s}^{-1}$. The uncertainty in k_c was determined as the range of k_c values that correspond to the maximum allowable deviation, which has been set as 3 times the minimum deviation ($\epsilon_{\min} = 2.5 \times 10^{-5}$). Using these guidelines, $k_c = 0.26 \pm 0.025 \text{ s}^{-1}$ and $k_u = 2.5 \pm 0.24 \text{ s}^{-1}$.

and each data point represents the average of a minimum of 400 simulations for a unique k_c/k_u pair. For increasing values of K_D , ϵ decreases until $K_D = 9.5$, after which ϵ increases again (as also demonstrated by Fig. 4). For $K_D = 9.5$, there is a parabolic relationship between ϵ and the individual k_c/k_u pairs and at $k_c = 0.26$, ϵ is minimized. The uncertainty in k_c was estimated as described in Materials and Methods from the data for $K_D = 9.5$. The maximum allowable deviation between simulation and experiment was set as 3 times the minimum deviation ($\epsilon_{\min} = 2.5 \times 10^{-5}$), from which the corresponding range for k_c was determined. Using these guidelines, $k_c = 0.26 \pm 0.025 \text{ s}^{-1}$ and $k_u = 2.5 \pm 0.24 \text{ s}^{-1}$.

Overall, the simulated WT integrin underwent directed transport $59.7 \pm 3.5\%$ of the time, with values of $k_c = 0.26 \text{ s}^{-1}$ and $k_u = 2.5 \text{ s}^{-1}$ ($K_D = 9.5$), compared to $60 \pm 13\%$ determined experimentally. Furthermore, the time-averaged velocity for the best-fit simulated case was $4.4 \pm 1.7 \mu\text{m}/\text{min}$ compared with the experimental value of $4.5 \pm 4.5 \mu\text{m}/\text{min}$.

Stochastic coupling model can simulate directed transport

Fig. 6 illustrates three simulated paths each for WT integrin $D = 3.5 \times 10^{-10} \text{ cm}^2/\text{s}$, $k_c = 0.26 \text{ s}^{-1}$, $k_u = 2.5 \text{ s}^{-1}$) and for pure diffusion ($D = 3.5 \times 10^{-10} \text{ cm}^2/\text{s}$, k_c and $k_u = 0$). The values for k_c and k_u were determined for the WT integrin by iteratively matching simulation results with experimental data as described in Materials and Methods and as outlined in Figs. 4 and 5. Panels A, C, and E in Fig. 6 illustrate paths for WT integrin and panels B, D, and F are trajectories for

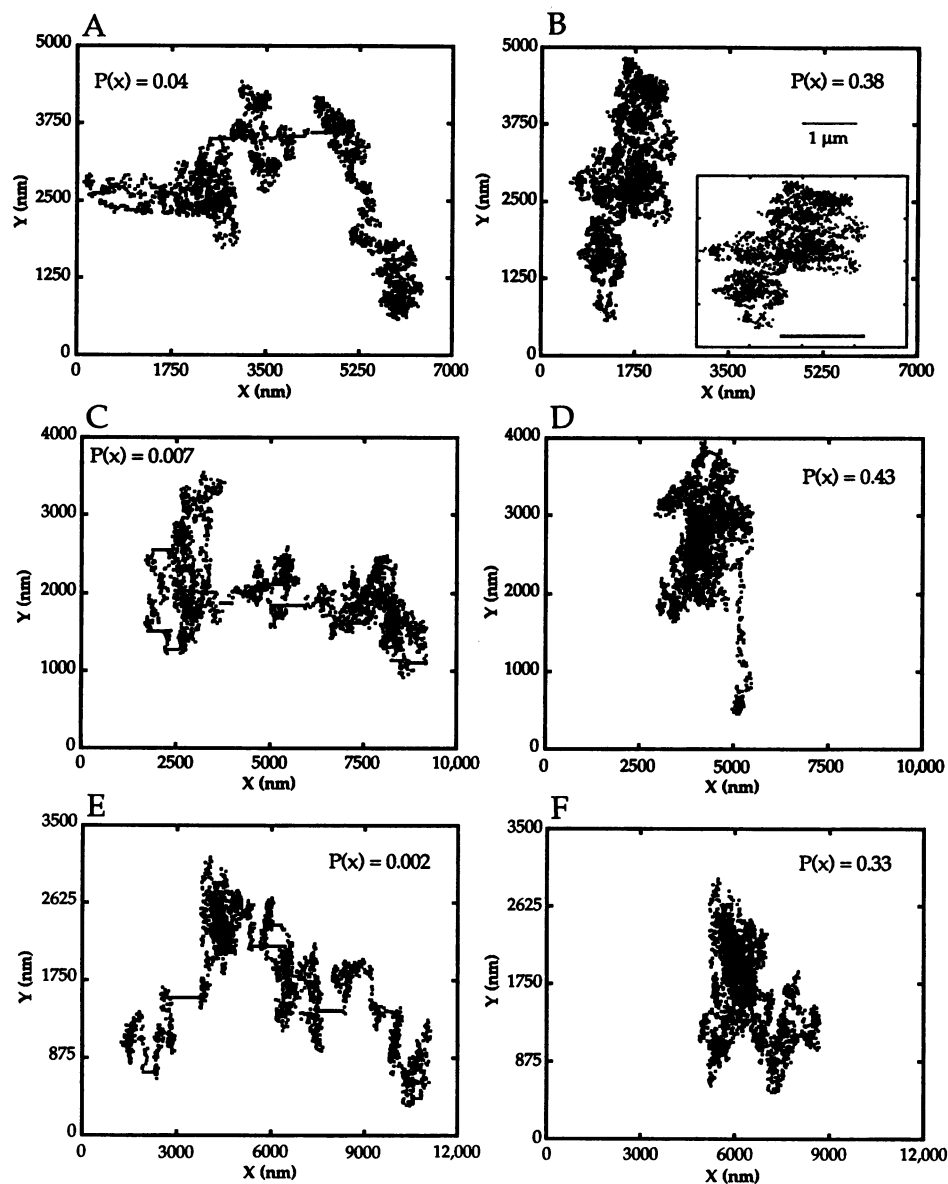


FIGURE 6 Simulated trajectories for integrin undergoing either directed transport or pure diffusion. Panels A, C, and E are three different simulated paths, each classified as directed ($P(x) < 0.05$), for integrin undergoing directed transport ($D = 3.5 \times 10^{-10} \text{ cm}^2/\text{s}$, $v_i = 37 \text{ } \mu\text{m}/\text{min}$, $k_c = 0.26 \text{ s}^{-1}$, $k_u = 2.5 \text{ s}^{-1}$) and panels B, D, and F are simulated diffusive trajectories ($D = 3.5 \times 10^{-10} \text{ cm}^2/\text{s}$, $v_i = 37 \text{ } \mu\text{m}/\text{min}$, k_c and $k_u = 0$). The inset, an enlargement of the path shown in panel B, illustrates the detailed character of the diffusive path. The scale bars in both panel B and the inset are $1 \text{ } \mu\text{m}$. The seeds used to initiate the random number generator within each simulation are -7491 (A, B), -53949 (C, D), and -36185 (E, F). Adjacent plots have identical scales for the x and y axes.

pure diffusion, with adjacent plots having the same axes scales. The seeds used to initiate the random number generator within each simulation are -7491 (A, B), -53949 (C, D), and -36185 (E, F). All three WT paths were scored as directed, $P(x) < 0.05$, and the three diffusion paths were categorized as diffusive, $P(x) \geq 0.05$, by the statistical criteria outlined in Materials and Methods. The directed nature and the brief, rapid excursions of the simulated WT integrin paths are quite noticeable compared to the paths for pure diffusion. In addition, the net displacement is considerably larger for integrin allowed to interact with the moving cytoskeletal element compared to the diffusion case. Note that in this figure, as well as in later figures, differences in the x and y scales yield diffusive plots that falsely appear skewed in the y -direction. The inset is the same diffusive path as for Fig. 6 B but with maximized x/y scales to illustrate the absence of any directed excursions and to demonstrate that diffusion is not oriented preferentially in the y -direction (scale bars in Fig. 6 B and the inset each represent $1 \text{ } \mu\text{m}$).

Fig. 1 illustrates analogous trajectories from the colloidal gold tracking experiments. The plots in Fig. 1 A, C, and E are paths, each classified as undergoing directed transport, for three different gold particles bound to WT integrin and panels B, D, and F illustrate different trajectories, all scored as diffusive, for beads attached to the truncated integrin (765t), which is unable to interact with the underlying cytoskeleton. Again, adjacent plots have identical scales for the x and y axes. As with the simulated paths, the directed nature of the experimental WT integrin paths is evident when compared with the paths for truncated integrin. In addition, the net displacement of integrin undergoing directed transport is larger than that for the pure diffusion case. The diffusive paths show no directed excursions (*inset*) and little net displacement of the integrin. The scale bars in Fig. 1 B and the inset each represent $1 \text{ } \mu\text{m}$.

Interestingly, $11 \pm 6\%$ of the simulated diffusive paths were scored as directed using our statistical criteria. As suggested by Saxton (1993), this nonbiased, two-dimensional

random walk serves as a control for estimating the error associated with the process of classifying paths as either directed or diffusive. Experimentally, we found that $17 \pm 16\%$ of the particles on the surface of untransfected cells underwent directed transport. We originally presumed that these directed cases represented nonspecific binding of the Ab-coated gold particles to membrane proteins undergoing directed transport (Schmidt et al., 1993). Instead, results from our simulations suggest that the directed transport cases observed for untransfected cells represent statistical background levels for our analysis rather than biochemical background levels for the experimental technique.

In addition, we determined that $7 \pm 9\%$ of particles bound to the truncated integrin, 765t, were classified as undergoing directed transport. This value is also consistent with the fraction of diffusive paths that are mistakenly identified as non-diffusive events according to our statistical criteria. These results further support the hypothesis that the truncated integrin diffuses in the membrane and, therefore, does not interact with a cytoskeletal component that could give rise to directed excursions.

Character of directed transport trajectories is sensitive to both K_D and k_c

Figs. 7 and 8 demonstrate the sensitivity of the simulated directed transport trajectories to changes in K_D and k_c , respectively. Fig. 7 illustrates simulated paths for K_D values of 1 (A), 9.5 (B), and 100 (C). In all three cases, the value for k_c is 0.26 s^{-1} (the obtained best-fit value). The character of the trajectory for $K_D = 100$ is essentially indistinguishable from a typical diffusive path (see Fig. 1 B, D, and F and Fig. 6 B, D, and F), whereas the representative path for $K_D = 1$ contains many lengthy directed excursions. Note that the scales for the three plots are not identical; the net displacement for $K_D = 1$ is much larger ($\sim 30,000 \text{ nm}$) than that for our best-fit case, $K_D = 9.5$. The net displacement observed for $K_D = 9.5$ ($\sim 10,000 \text{ nm}$) is similar to that observed experimentally (avg. $\sim 7000\text{--}12,000 \text{ nm}$). For $K_D = 1$, an average of 100 trajectories yielded $\%Dir = 100$ and $\langle v \rangle = 18 \mu\text{m}/\text{min}$, whereas for $K_D = 100$, $\%Dir = 8$ and $\langle v \rangle = 4 \mu\text{m}/\text{min}$. Recall that we experimentally found $\%Dir = 60$ and $\langle v \rangle = 4.5 \mu\text{m}/\text{min}$, and simulations for our best-fit case ($K_D = 9.5$, $k_c = 0.26 \text{ s}^{-1}$) yielded $\%Dir = 59.7$ and $\langle v \rangle = 4.4 \mu\text{m}/\text{min}$.

Fig. 8 depicts simulated trajectories for k_c values of 0.03 s^{-1} (A), 0.26 s^{-1} (B), and 3 s^{-1} (C). For all three paths, $K_D = 9.5$ (the obtained best-fit value). The path for $k_c = 0.03 \text{ s}^{-1}$ has a more overall diffusive character compared to the path for $k_c = 0.26 \text{ s}^{-1}$. In general, the value for k_c (0.03 s^{-1}) is small such that integrin, under this condition, has a much lower probability of linking to the moving cytoskeleton. However, when integrin does link to the cytoskeletal element, it remains attached for a longer period of time because of the correspondingly low value for k_u (as evidenced by the very long directed excursion in Fig. 8 A). On the other hand, the trajectory for $k_c = 3 \text{ s}^{-1}$ suggests that integrin, under this

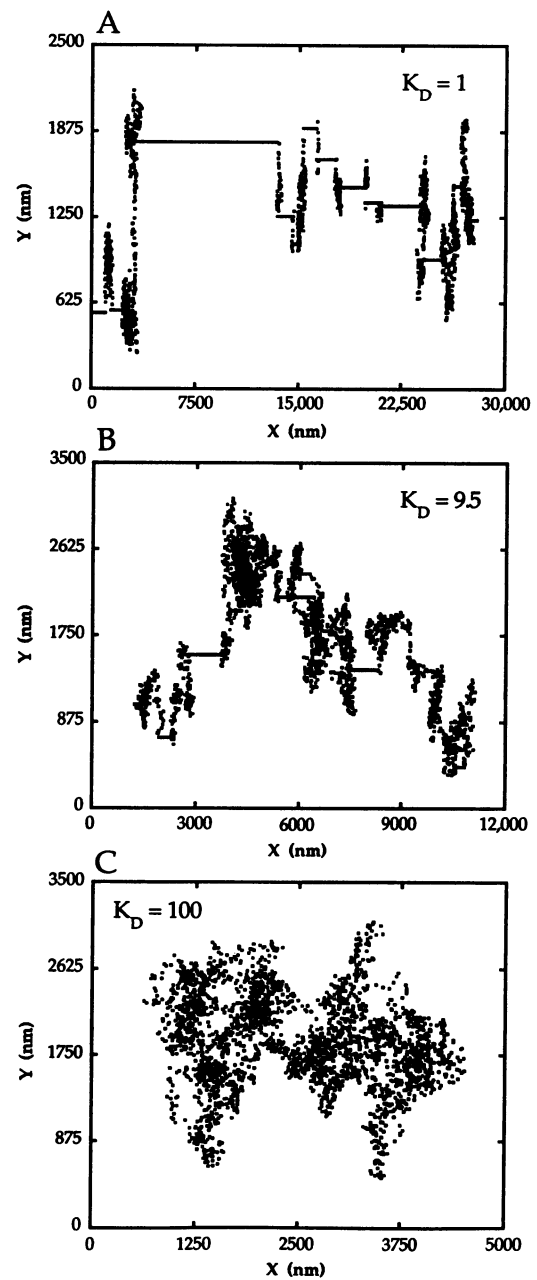


FIGURE 7 Sensitivity of simulated integrin trajectories to changes in K_D . This figure illustrates simulated paths for K_D values of 1 (A), 9.5 (B), and 100 (C). In all three cases, the value for k_c is 0.26 s^{-1} (the obtained best-fit value), $D = 3.5 \times 10^{-10} \text{ cm}^2/\text{s}$, and $v_i = 37 \mu\text{m}/\text{min}$. For $K_D = 100$, $k_u > 3 \text{ s}^{-1}$ and the simplified equation, $P_u = k_u \Delta t$, is not accurate. Rather, for this case and as described in Appendix A, the rigorous expression, $P_u = 1 - \exp(-k_u \Delta t)$ was used in the simulation program. The probabilities that diffusion could give rise to the net displacement, x , for the three paths are: (A) $P(x) = 1 \times 10^{-6}$, (B) $P(x) = 0.002$, and (C) $P(x) = 0.6$. Recall that for $P(x) < 0.05$ the path is scored as directed and for $P(x) \geq 0.05$ the path is considered diffusive. Note that the scales for the three plots are not identical.

fabricated condition, interacts readily with the moving cytoskeletal element, as judged by the overall directed path. However, the uncoupling rate constant is also large ($k_u = 28.5 \text{ s}^{-1}$) resulting in the dissociation of integrin from the cytoskeleton

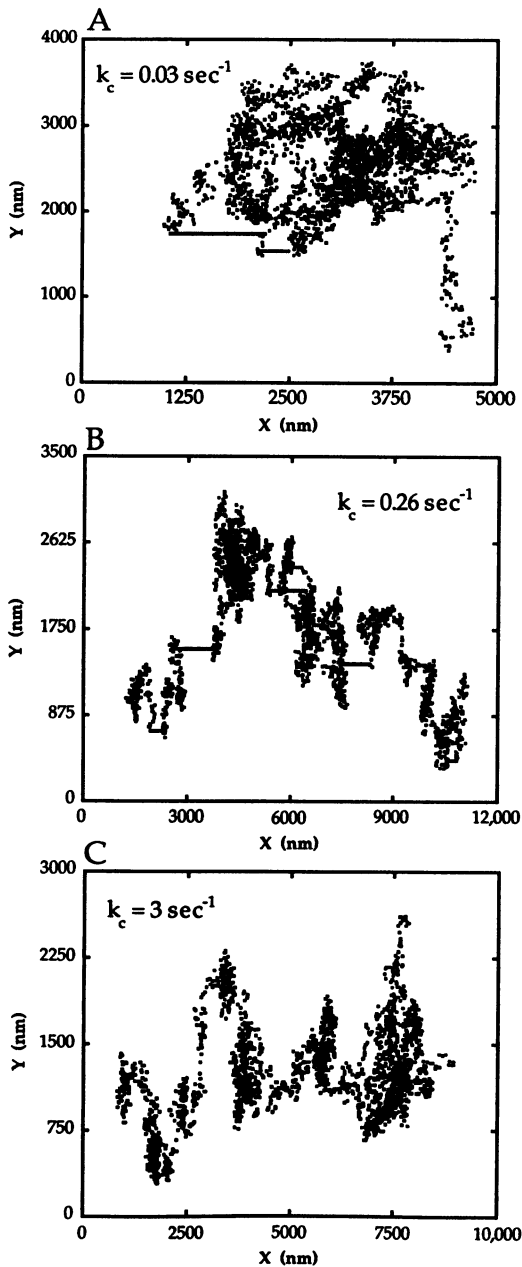


FIGURE 8 Sensitivity of simulated integrin trajectories to changes in k_c . This figure illustrates simulated paths for k_c values of 0.03 s^{-1} (A), 0.26 s^{-1} (B), and 3 s^{-1} (C). For all three paths, $K_D = 9.5$ (the obtained best-fit value), $D = 3.5 \times 10^{-10} \text{ cm}^2/\text{s}$, and $v_i = 37 \text{ }\mu\text{m}/\text{min}$. For $k_c = 3 \text{ s}^{-1}$, $k_u > 3 \text{ s}^{-1}$ and the simplified equation, $P_u = k_c \Delta t$, is not accurate. As described in Appendix A, the rigorous expression, $P_u = 1 - \exp(-k_u \Delta t)$ was used for this case in the simulation program. The probabilities that diffusion could give rise to the net displacement, x , for the three paths are: (A) $P(x) = 0.3$, (B) $P(x) = 0.002$, and (C) $P(x) = 0.03$. Note that the scales for the three plots are not identical.

immediately after its linkage. The result is an overall directed path with no obvious directed excursions in the $+x$ direction. In fact, no directed excursions were observed in multiple analyzed trajectories for $k_c = 3 \text{ s}^{-1}$. For $k_c = 0.26 \text{ s}^{-1}$ (the obtained best-fit value), we observed paths having short directed excursions as well as a rapid association/dissociation

character similar to that observed for $k_c = 3 \text{ s}^{-1}$. Experimentally, we found paths with a character similar to that for $k_c = 3 \text{ s}^{-1}$ (Fig. 1 B), but most did have obvious, brief rapid excursions as found for $k_c = 0.26 \text{ s}^{-1}$ (Fig. 1, A and C). For $k_c = 0.03 \text{ s}^{-1}$, an average of 100 trajectories yielded $\%Dir = 43$ and $\langle v \rangle = 8 \text{ }\mu\text{m}/\text{min}$, whereas for $k_c = 3 \text{ s}^{-1}$, $\%Dir = 91$ and $\langle v \rangle = 5 \text{ }\mu\text{m}/\text{min}$. In contrast, our best-fit case ($K_D = 9.5$, $k_c = 0.26 \text{ s}^{-1}$) yielded $\%Dir = 59.7$ and $\langle v \rangle = 4.4 \text{ }\mu\text{m}/\text{min}$, which corresponds most closely with our experimental observations, $\%Dir = 60$ and $\langle v \rangle = 4.5 \text{ }\mu\text{m}/\text{min}$.

Integrin-cytoskeleton interactions are fast compared to other reactions

The forward rate constant for integrin-cytoskeleton coupling, k_c , has units of s^{-1} and, therefore, has implicitly included in it a local concentration of the associating cytoskeletal element. Thus, it really should be considered as an apparent rate constant. Because this element is unidentified and its concentration is unknown, it is difficult to compare the coupling rate constant for this interaction with other reaction rate constants.

However, the rate constant for integrin-cytoskeleton uncoupling, k_u , does not depend on the surrounding concentration for the cytoskeleton, permitting its value to be compared with reverse rate constants for other reactions. In fact, k_u for integrin ($k_u = 2.5 \text{ s}^{-1}$) is fast compared with some typical reverse rate constants, k_r , for other reactions. For example, $k_r = 0.01 \text{ s}^{-1}$ for integrin/fibronectin interactions for fibroblasts, which is typically considered a low affinity association (Akiyama and Yamada, 1985; Table 2-1 in Lauffenburger and Linderman, 1993). The rate constant for the actin depolymerization process, $k_- = 1.4 \text{ s}^{-1}$ (Amos and Amos, 1991), is numerically closest to our observed value for the integrin-cytoskeleton interactions that give rise to directed transport.

Directed transport is likely a diffusion-limited process

For reactions involving membrane molecules, the coupling and uncoupling rate constants, k_c and k_u , are effective values that reflect the intrinsic rate constants, k_{on} and k_{off} , and a diffusion effect (Lauffenburger and Linderman, 1993). In other words, interacting species must first diffuse through the membrane to encounter each other before coupling can proceed at its intrinsic velocity.

The rate constants determined from the simulations for integrin-cytoskeleton interactions were compared with an equivalent rate constant for diffusion, k_+ , to determine the rate-limiting step for the directed transport process (Appendix B). We assumed that integrin is diffusing with an average diffusivity of $D = 3 \times 10^{-10} \text{ cm}^2/\text{s}$ and that the total number of reactive cytoskeletal elements, the identity of which is unknown, is of similar magnitude as the total number of integrins on the cell surface, $10^5/\text{cell}$ (Akiyama and Yamada, 1985; Sczekan and Juliano, 1990). We found that the equivalent diffusion rate constant for integrin, $k_+ = 0.36 \text{ s}^{-1}$, would

be limiting for the overall coupling rate constant for integrin, $k_c = 0.26 \text{ s}^{-1}$. In other words, because $k_c \approx k_+$, the directed transport process is diffusion-limited and an intrinsic value for k_{on} cannot be determined.

For numbers of cytoskeletal elements greater than $10^5/\text{cell}$, the overall directed transport of integrin is not limited by the diffusion of integrin to an available cytoskeletal element, but rather is limited by the intrinsic rate of coupling between integrin and the cytoskeleton. For example, for $N = 10^6$, then $k_+ = 5 \text{ s}^{-1}$, which is over an order of magnitude larger than k_c . However, the previous estimates for k_+ assume that the cytoskeletal element is evenly distributed throughout the cell and that all of these elements are free to interact with integrin, which is presumably not the case. For these reasons, we believe that the directed transport of integrin is most likely diffusion-limited, which is typical of most membrane reactions.

Directed transport is necessary for formation of nascent adhesions

An important question is whether directed transport is required for the delivery of integrin to the cell's leading edge where nascent adhesions are formed. If diffusion alone is sufficient to supply a majority of integrins to the cell front in a required time, then the role that directed transport plays in cell migration would be questionable.

Calculations for the movement of integrin across the leading lamella ($\sim 10 \mu\text{m}$) by diffusion versus directed transport indicate that interaction of integrin with a moving cytoskeletal element significantly reduces the transport time (Appendix C). Integrin diffusing with an average diffusivity of $3 \times 10^{-10} \text{ cm}^2/\text{s}$ would require approximately 28 min to reach the leading edge, whereas integrin that is undergoing directed transport, with a time-averaged velocity of $4 \mu\text{m}/\text{min}$, requires only 3 min. Therefore, the additional velocity in the direction toward the leading edge reduces the transport time by roughly an order of magnitude.

Previous live cell fluorescence studies with migrating chicken fibroblasts demonstrated that new contacts can form at the leading edge within 10 min of lamellipodal extension (Regen and Horwitz, 1992). This strongly suggests that directed transport is necessary to supply large numbers of integrins to the leading edge within a reasonable time to allow for contact formation.

Our calculations assume that the transport of integrin occurs after the leading lamella has fully extended and that all integrins originate at the base of the lamella. Some integrins on the cell front are likely carried forward passively with the extending membrane during the motile cycle. However, most integrins in the advancing portion of the cell participate in the formation of nascent adhesions, which move rearward relative to the cell frame of reference, therefore resulting in a relative depletion of integrin at the cell front (Regen and Horwitz, 1992). As a result, a significant number of integrins are probably not carried forward with the extending membrane. Our assumption that most integrins must traverse the

entire leading lamella is also consistent with the observation that microtubules insert behind the lamella (Amos and Amos, 1991). Therefore, newly synthesized or recycled integrins, which are transported in vesicles along the microtubule network, will insert in the membrane at the base of the leading lamella and then must be carried to the cell's leading edge by another mechanism. These data further support our claim that an external mechanism such as directed transport is likely necessary to provide integrins to the advancing region of the cell where new contacts are formed.

DISCUSSION

Cell migration is a phenomenon requiring dynamic adhesive interactions between the internal motile machinery and the external substratum, with adhesion receptors, such as integrins, serving as the transmembrane link. New adhesions within the migrating cell form at the cell's leading edge and either release or rip at the cell rear (Regen and Horwitz, 1992). Some evidence suggests the possibility for the recycling of integrins to the cell front (Bretscher, 1989), but other research argues that vesicles containing integrins are not present in the cell's leading lamella (Regen and Horwitz, 1992). Work by Kucik et al. (1989) demonstrated that membrane glycoproteins (bound by 40 nm gold beads) are preferentially transported to the leading edges of migrating fish keratocytes by directed excursions interspersed with diffusion. This work suggested the possibility of a surface mechanism for the delivery of proteins, and possibly adhesion receptors, to critical sites within the migrating cell. The cytoskeleton was speculated as involved in this transport, but little proof existed to confirm this hypothesis. In our previous work, we used video microscopy and image analysis to demonstrate that integrin, an adhesion receptor shown to be critical for cell migration, is rapidly and intermittently transported forward on migrating mouse fibroblasts (Schmidt et al., 1993). The observed rapid, directed motions were statistically distinct from diffusion and could likely play a physiological role in cell migration by providing integrins to the cell's advancing edge where new adhesions are formed. Furthermore, we used cells transfected with $\beta 1$ integrins mutated by various degrees to show that directed transport requires the cytoplasmic domain of integrin. In particular, results for a cytoplasmic domain truncation mutant and single amino acid mutants demonstrate that directed transport involves the coupling of integrin to a moving cytoskeletal component that gives rise to directed transport.

In the present work, we have written a computer program to simulate the diffusive as well as directed nature of integrin transport to the cell's leading edge. This model assumes that integrin either diffuses in the cell membrane with a known diffusivity (D) or transiently couples to a cytoskeletal element moving with a known velocity (v_i). By comparing the simulated trajectories with those obtained experimentally, we were able to determine the coupling and uncoupling rate constants for the interaction of integrin with cytoskeletal elements *in vivo* ($k_c = 0.26 \pm 0.025 \text{ s}^{-1}$ and $k_u = 2.5 \pm 0.24$

s^{-1} , respectively). Comparison of these rate constants with an equivalent rate constant for diffusion indicates that the coupling interaction is likely a diffusion-limited process, which is expected for membrane processes. We have also shown by calculation that directed transport is necessary for integrin to traverse the length of an extending lamellipod to the leading edge; i.e., diffusion alone cannot account for the delivery of integrin to areas where new adhesions form.

Our simulation results, which accurately depict experimental data, further support the hypothesis that integrin is interacting transiently with a moving cytoskeletal element that gives rise to the forward motion of integrin. However, the precise molecules and mechanisms involved in this phenomenon are still unknown. The $\beta 1$ subunit of integrin has been shown to interact *in vitro* with the cytoskeletal proteins α -actinin and talin (Otey et al., 1990; Horwitz et al., 1986) and, to date, there exists no conclusive evidence for interactions of the α subunit of integrin with the cytoskeleton, suggesting that this function relies predominantly upon the β subunit (Solowska et al., 1989; Hayashi et al., 1990; LaFlamme et al., 1992). The cytoskeletal proteins α -actinin and talin can interact either directly or indirectly with the actin cytoskeleton, providing a linkage between integrin and the actin-based motor.

Therefore, the directed transport of integrin likely arises from a linkage to the actin cytoskeleton (the involvement of other linkage proteins besides α -actinin and talin might be a possibility). Yet, in general, the actin cytoskeleton is undergoing a centripetal flow or treadmilling (Wang, 1985; Okabe and Hirokawa, 1989; Symons and Mitchison, 1991) that gives rise to the slow, rearward motion of crosslinked membrane proteins, including integrins (Harris and Dunn, 1972; Dembo and Harris, 1981; Fisher et al., 1988; Schmidt et al., 1993). So how can rearward moving actin produce a forward, directed transport of bound proteins? A hypothesis for such a mechanism was described by Sheetz et al. (1990), who suggested that uncross-linked membrane proteins (e.g., integrin) can associate with a subset of short actin filaments that are not undergoing centripetal, rearward movement. These short actin filaments are subsequently directed forward by a myosin I analog that moves along the underlying, continuous actin filament network toward the + (polymerizing) ends near the cell front. The affinity of myosin I for lipids (Adams and Pollard, 1989) could maintain the short actin filaments near the cell surface. This hypothesis for directed transport is further supported by the localization of myosin I almost exclusively at the front edges of motile cells (Fukui et al., 1989). Other potential hypotheses for the mechanisms governing membrane protein dynamics are outlined by Sheetz (1993). Thus, the actin cytoskeleton, in combination with unique linker proteins and motor proteins, can give rise to two classes of behavior for integrins: (1) a slow rearward movement of large aggregates of integrin bound to actin filaments undergoing a centripetal motion; and (2) a rapid transport of uncross-linked integrins possibly interacting with short actin filaments that are moved forward by myosin I-like proteins. The slow rearward motion could give

rise to cell locomotion by allowing intracellular force to be transmitted as a traction force along the substrate through integrin-mediated adhesions. The rapid transport likely serves to deliver integrins to the cell periphery where new adhesions are formed.

Integrin-cytoskeleton interactions that give rise to directed transport were found from our dynamic coupling model to be very fast ($k_c = 0.3 s^{-1}$, $k_u = 3 s^{-1}$) in comparison with other reactions. For example, $k_r = 0.01 s^{-1}$ for integrin/fibronectin interactions in fibroblasts (Akiyama and Yamada, 1985). A possible rationale for the rapid interactions is to prevent integrin from being bound for extended periods to the subset of short actin filaments. When integrin reaches the leading edge, it could then easily associate with other integrins and matrix molecules to form nascent adhesions and subsequently bind to the underlying, rearward moving actin filaments to allow for cell locomotion.

Knowledge of the time-scales for integrin-cytoskeleton interactions could potentially be useful for selecting and engineering molecules that will inhibit integrin-cytoskeletal interactions in the moving cell or for incorporation into mechanistic models describing integrin-based adhesion or migration processes for cells. For example, the mechanistic model of DiMilla et al. (1991) describes cell migration in terms of interactions between integrin and its matrix molecules. However, the linkage of integrin to the cytoskeleton motor is assumed, but not accounted for, in any molecular detail. In addition, the supply of integrin to adhesions by a mechanism other than diffusion is not accounted for in this model. As a second example, the theoretical analysis of Ward and Hammer (1993) describes the effects of focal contact formation (large aggregates of integrin in close association with both matrix components and the actin cytoskeleton) on cell-substrate adhesion strength. These authors treat the integrin-cytoskeleton interaction as an equilibrium process because their interest is in the strength of the final structure. Our estimated *in vivo* rate constants for integrin's interaction with the cytoskeleton can ultimately be incorporated into mechanistic models such as these to yield a more complete dynamic understanding of integrin-mediated adhesion and migration.

A major assumption in our dynamic coupling model is the unidirectional motion of the cytoskeletal element toward the cell's leading edge (+ x direction), which is justified by the experimental observations that directed motions occur predominantly in one direction (Kucik et al., 1989; Schmidt et al., 1993). Our assumption is also consistent with the discovery that actin filaments in the lamella, along which myosin I could move, align parallel to the direction of motion (Bearer, 1989). However, our assumption for unidirectional excursions could potentially be relaxed in the model, allowing for directed motions in any direction (360°) or toward the leading edge, but at an angle (180°). Permitting directed motions randomly in any direction will yield simulated trajectories statistically indistinguishable from diffusion. Unlike diffusion, rapid excursions will be observed because the integrin can link to the cytoskeleton for brief periods of time,

but these randomly oriented excursions will cancel, resulting in little or no net displacement. On the other hand, directed motions toward the leading edge within a 180° radius will produce net displacements larger than for pure diffusion, but likely smaller than those observed for unidirectional motion. For a given k_c/k_u pair, the length of each directed excursion will be the same for the unidirectional and 180° cases, but the excursions for the 180° case will not effect as large a net displacement because they will be randomly positioned within a half circle. Thus, for the 180° case, to match simulation to experiment, we predict that smaller values for K_D would be required to yield experimentally measured displacements and %Dir. In other words, more or lengthier directed excursions for the 180° case, compared to the unidirectional case, would be necessary for integrin to traverse the required distance on the cell lamellipod. However, large numbers of directed excursions would yield a greater value for the time-averaged velocity for directed transport, compared to that obtained experimentally. This discrepancy between the predicted simulation outcome for the 180° case and our experimental observations further justifies our original assumption for unidirectional motion of the cytoskeletal element.

Other parameters that may play roles in directed transport, but that are not explicitly addressed in our coupling model, include (1) matrix molecules and (2) integrin-integrin interactions. The binding of matrix molecules to integrin has not been accounted for to any extent in our dynamic coupling model. The monoclonal antibody that we used in our previous colloidal gold tracking experiments (Schmidt et al., 1993) was nonadhesion-perturbing (i.e., the antibody does not interact with the matrix-binding domain of the integrin), indicating that fibronectin (or vitronectin or laminin) could in fact have been bound to the integrins undergoing directed transport. Therefore, additional experiments would need to be performed to clarify the role of matrix molecules in the directed transport of integrin. However, with our model, we are interested in understanding the interactions of integrin with the cytoskeleton, regardless of the factors necessary to convert integrin to its "active" state. For similar reasons, we have not accounted for potential integrin-integrin interactions. The integrin in our model may not necessarily represent a single receptor, but may in fact characterize the behavior of a small aggregate of integrins. In this case, our rate constants are effective values that reflect the dynamics of a more complex process. As detailed under Materials and Methods, we used experimental techniques to demonstrate that various degrees of aggregation for integrins (and single integrins, if we "extrapolate" to a single antibody per contact site on the gold particles) do not significantly affect the directed transport of this molecule. This suggests that the directed transport process, either of single integrins or of small clusters, is a physiologically real event, such that the dynamics of the overall transport process is more informative than intrinsic kinetics for a single integrin event.

We are grateful to Kim Forsten, Alan Horwitz, and Michael Sheetz for helpful discussions, and to Dane Wittrup for a critical review of the manuscript.

This work was supported by a Johnson & Johnson Focused Giving Award to D. A. Lauffenburger.

APPENDIX A

Probabilities for coupling and uncoupling

The probability that integrin will uncouple, P_u , during a given time, Δt , interval is rigorously written as

$$P_u = 1 - \exp(-k_u \Delta t), \quad (\text{A1})$$

where k_u is the uncoupling rate constant in s^{-1} . Eq. A1 is derived from a first-order reaction, assuming that a single integrin can undergo only a single binding step within a small time interval. Expansion of Eq. A1 in a Taylor series yields

$$P_u = k_u \Delta t - (k_u \Delta t)^2/2! + \dots \quad (\text{A2})$$

For small values of $k_u \Delta t$, Eq. A2 is accurately represented by the simplified form

$$P_u = k_u \Delta t. \quad (\text{A3})$$

Analogously, for the coupling process,

$$P_c = k_c \Delta t, \quad (\text{A4})$$

where k_c is the coupling rate constant (s^{-1}) and P_c is the probability of integrin coupling to the cytoskeleton within a single time interval.

In all of our simulations, $\Delta t = 1/30$ s. For values of k_c or k_u up to $3 s^{-1}$, the error between the rigorous result for the corresponding probability (Eq. A1 and an analogous equation for P_c) and the simplified value (Eqs. A3 and A4) is less than 5%. Therefore, to simplify calculations, Eqs. A1 and A2–A3 were used within the simulation program for values of k_c or $k_u < 3 s^{-1}$. For larger values of k_c and k_u , and where specified, the exact form for the probability (Eq. A1 and an analogous equation for P_c) was used.

APPENDIX B

Diffusion effects on directed transport

Diffusive transport is characterized by the rate constant k_+ , and the intrinsic rate constants for coupling and uncoupling are k_{on} and k_{off} . Comparison of k_+ to k_{on} and k_{off} gives an indication of the rate-limiting step for the entire coupling process. As an example, the dependence of k_c on k_{on} and k_+ is represented as

$$\frac{1}{k_c} = \frac{1}{k_+} + \frac{1}{k_{on}} \quad (\text{B1})$$

$$k_c = (1/k_+ + 1/k_{on})^{-1}. \quad (\text{B2})$$

As depicted in Eq. B1, the relationship between the rate constants can be written as a series of resistances ($1/k$) in which the rate for the overall coupling process is inversely proportional to the sum of the resistances provided by diffusion and the intrinsic reaction.

The diffusion rate constant (k_+) was previously derived by Lauffenburger and Linderman (1993) for a membrane molecule as

$$k_+ = \frac{2\pi D}{\ln(b/s)}, \quad (\text{B3})$$

where D is the diffusivity of the membrane molecule, b is one-half the mean distance between a given number of species available for reaction, and s is the encounter radius for reaction. The value for b can be approximated from the relation $A = N\pi b^2$, where A is the surface area of the cell and N is the

total number species available for reaction (here, the cytoskeleton). For the cells used in our previous experiments, A is about $10^4 \mu\text{m}^2$ (10^{-4}cm^2), as estimated experimentally from videotape. The species with which integrin interacts for directed transport has not been identified, so the number of these species available for reaction with integrin, N , is not known. Our best guess is to assume that the number of cytoskeletal elements available for reaction is roughly equal to the number of integrins on the cell surface, $N = 10^5/\text{cell}$ (Akiyama and Yamada, 1985; Sczekan and Juliano, 1990). These values, in addition to $D = 3 \times 10^{-10} \text{cm}^2/\text{s}$ and $s = 10^{-7} \text{cm}$ (Lauffenburger and Linderman, 1993), yield $b = 2 \times 10^{-5} \text{cm}$ and $k_+ = 3.6 \times 10^{-10} \text{cm}^2/\text{s}$.

To compare this to k_c , the units for k_+ need to be converted to s^{-1} :

$$k_+ (\text{s}^{-1}) = \frac{k_+ (\text{cm}^2/\text{s}) * 10^5 (\#/\text{cell})}{10^{-4} (\text{cm}^2/\text{cell})} \quad (\text{B4})$$

From Eq. B4 we find that for $N = 10^5/\text{cell}$, $k_+ = 0.36 \text{s}^{-1}$, which is essentially indistinguishable from $k_c = 0.26 \text{s}^{-1}$ for integrin. Because $k_c \approx k_+$, the directed transport process is diffusion-limited, which is typical for membrane reactions (Lauffenburger and Linderman, 1993). If we solve Eqs. B3 and B4 using $N = 10^4$ and 10^6 , because the value for N is not known, we find that $k_+ = 0.03 \text{s}^{-1}$ and 5s^{-1} , respectively. For 10^4 cytoskeletal components available for interaction with integrin, the overall coupling process is diffusion-limited. On the other hand, for $N = 10^6$, $k_+ > k_c$, indicating that the intrinsic coupling reaction is the rate-limiting step for directed transport. In other words, for reaction-limited coupling, diffusion of the interacting species to each other is relatively fast, and the rate for the overall coupling process is determined by the intrinsic reaction rate, $k_c \approx k_{\text{on}}$. However, these estimated values for k_+ assume that the cytoskeletal element is evenly distributed within the cell and that all cytoskeletal elements are free to interact with integrin, which is likely not the case. Therefore, for these reasons, we believe that the directed transport phenomenon is probably a diffusion-limited process, which is typical of most membrane reactions.

Other derivations of Eq. B4 are similar except that a constant, C , is subtracted from $\ln(b/s)$ in the denominator. Values for C range from $G = 0.231$ (Keizer, 1985) to $C = 0.75$ (Berg and Purcell, 1977). Even for the most extreme value of C (0.75), $k_+ = 0.42 \text{s}^{-1}$ for integrin with $N = 10^5$, which does not differ significantly from $k_c = 0.26 \text{s}^{-1}$.

APPENDIX C

Time required for diffusion versus directed transport to leading edge

The time for unidirectional (one-dimensional) transport of the integrin across the distance of the lamella was calculated for purely diffusing integrin and integrin undergoing directed transport. The lamella is assumed to be $10 \mu\text{m}$ (estimated experimentally from video tape), and an average diffusivity of $3 \times 10^{-10} \text{cm}^2/\text{s}$ and the average time-averaged velocity for directed transport of $4 \mu\text{m}/\text{min}$ (determined experimentally from parallel MSD versus time plots) were used. For a molecule diffusing in one dimension, the relationship between the displacement, Δx , of the molecule and its diffusivity, D , is given by

$$\langle \Delta x^2 \rangle = MSD = 2D\Delta t, \quad (\text{C1})$$

where Δt is the time interval over which the molecule has diffused. For a molecule that is diffusing and simultaneously subjected to an external velocity, the equivalent expression is

$$MSD = 2D\Delta t + \langle v \rangle^2 \Delta t^2 \quad (\text{C2})$$

where v is the time-averaged velocity due to the external force.

If Eq. C1 is solved for Δt with $D = 3 \times 10^{-10} \text{cm}^2/\text{s}$ and $\Delta x = 10 \mu\text{m}$, we find that a time of 28 min is necessary for integrin to diffuse to the cell's leading edge. Solving Eq. C2 with D and Δx the same as above and with $\langle v \rangle = 4 \mu\text{m}/\text{min}$ yields a time of 3 min for transport of integrin to the cell front.

For these calculations, we have assumed that integrin originates at the base of the lamella (point where microtubules insert). In addition, it is as-

sumed that transport occurs after the lamellipod has fully extended (to neglect effects of membrane flow).

REFERENCES

- Adams, R., and T. D. Pollard. 1989. Binding of myosin I to membrane lipids. *Nature*. 340:565–568.
- Amos, L. A., and W. B. Amos. 1991. *Molecules of the Cytoskeleton*. Guilford Press, New York. 51–104.
- Akiyama, S. K., and K. M. Yamada. 1985. The interaction of plasma fibronectin with fibroblastic cells in suspension. *J. Biol. Chem.* 260:4492–4500.
- Bearer, E. 1989. Platelet membrane skeleton revealed by quick-freeze deep-etch. *Anat. Rec.* 228:1–11.
- Berg, H. C. 1983. *Random Walks in Biology*. Princeton University Press, Princeton, NJ. 14–16.
- Berg, H. C., and E. M. Purcell. 1977. Physics of chemoreception. *Biophys. J.* 20:193–219.
- Bretscher, M. S. 1989. Endocytosis and recycling of the fibronectin receptor in CHO cells. *EMBO J.* 8:1341–1348.
- Burridge, K., K. Faith, T. Kelly, G. Nuckolls, and C. Turner. 1988. Focal adhesions: transmembrane junctions between the extracellular matrix and the cytoskeleton. *Annu. Rev. Cell Biol.* 4:487–525.
- Cima, L. G., J. P. Vacanti, C. Vacanti, D. Ingber, D. Mooney, and R. Langer. 1991. Tissue engineering by cell transplantation using degradable polymer substrates. *J. Biomech. Eng.* 113:143–151.
- Croxton, F. E. 1953. *Elementary Statistics with Applications in Medicine and the Biological Sciences*. Dover Publications, Inc., New York. 259–265.
- Dembo, M., and A. Harris. 1981. Motion of particles adhering to the leading lamella of crawling cells. *J. Cell Biol.* 91:528–536.
- DiMilla, P. A., K. Barbee, and D. A. Lauffenburger. 1991. Mathematical model for the effects of adhesion and mechanics on cell migration speed. *Biophys. J.* 60:15–37.
- Dongarra, J. J., C. B. Moler, J. R. Bunch, and G. W. Stewart. 1979. *LINPACK User's Guide*. SIAM, Philadelphia, PA. 1.1–1.26.
- Fisher, G. W., P. L. Conrad, R. L. DeBiasio, and D. L. Taylor. 1988. Centripetal transport of cytoplasm, actin and the cell surface in lamellipodia of fibroblasts. *Cell Motil. Cytoskel.* 11:235–247.
- Fukui, Y., T. J. Lynch, H. Brazeska, and E. D. Korn. 1989. Myosin I is located at the leading edges of locomoting Dictyostelium amoebae. *Nature (Lond.)*. 341:328–331.
- Gelles, J., B. J. Schnapp, and M. P. Sheetz. 1988. Tracking kinesin-driven movements with nanometre-scale precision. *Nature (Lond.)*. 331:450–453.
- Harris, A., and G. Dunn. 1972. Centripetal transport of attached particles on both surfaces of moving fibroblasts. *Exp. Cell Res.* 73:519–523.
- Heidemann, S. R., P. Lamoureux, and R. E. Buxbaum. 1990. Growth cone behavior and production of traction force. *J. Cell Biol.* 111:1949–1957.
- Horwitz, A., K. Duggan, C. Buck, M. C. Beckerle, and K. Burridge. 1986. Interaction of plasma membrane fibronectin receptor with talin—a transmembrane linkage. *Nature (Lond.)*. 320:531–532.
- Keizer, J. 1985. Theory of rapid bimolecular reactions in solution and membranes. *Accounts Chem. Res.* 18:235–241.
- Kucik, D. F., E. L. Elson, and M. P. Sheetz. 1989. Forward transport of glycoproteins on leading lamellipodia in locomoting cells. *Nature (Lond.)*. 340:315–317.
- Lauffenburger, D. A., and J. J. Linderman. 1993. *Receptors: Models for Binding, Trafficking, and Signaling* Vol. 30. Oxford University Press, New York. 151–153.
- McCammon, J. A. 1991. Computer-aided molecular design. *Science (Washington DC)*. 238:486–491.
- Okabe, S., and N. Hirokawa. 1989. Incorporation and turnover of biotin-labeled actin microinjected into fibroblastic cells: an immunoelectron microscope study. *J. Cell Biol.* 109:1582–1595.
- Otey, C. A., F. M. Pavalko, and K. Burridge. 1990. An interaction between α -actinin and the $\beta 1$ integrin subunit in vitro. *J. Cell Biol.* 111:721–729.
- Press, W. H., B. P. Flannery, S. A. Teukolsky, and W. T. Vetterling. 1986.

- Numerical Recipes: The Art of Scientific Computing (FORTRAN Version). Cambridge University Press, Cambridge, MA. 24–29, 196, 203, 508–529.
- Regen, C. M., and A. F. Horwitz. 1992. Dynamics of $\beta 1$ integrin-mediated adhesive contacts in motile fibroblasts. *J. Cell Biol.* 119:1347–1359.
- Saxton, M. J. 1993. Lateral diffusion in an archipelago: single-particle diffusion. *Biophys. J.* 64:1766–1780.
- Sczekan, M. M., and R. L. Juliano. 1990. Internalization of the fibronectin receptor is a constitutive process. *J. Cell. Phys.* 142:575–580.
- Schmidt, C. E., A. F. Horwitz, D. A. Lauffenburger, and M. P. Sheetz. 1993. Integrin-cytoskeletal interactions in migrating fibroblasts are dynamic, asymmetric, and regulated. *J. Cell Biol.* 123:977–991.
- Sheetz, M. P., S. Turney, H. Qian, and E. L. Elson. 1989. Nanometre-level analysis demonstrates that lipid flow does not drive membrane glycoprotein movements. *Nature (Lond.)* 340:284–288.
- Sheetz, M. P., N. L. Baumrind, D. B. Wayne, and A. L. Pearlman. 1990. Concentration of membrane antigens by forward transport and trapping in neuronal growth cones. *Cell* 61:231–241.
- Sheetz, M. P. 1993. Glycoprotein motility and dynamic domains in fluid plasma membranes. *Annu. Rev. Biophys. Biomol. Struct.* 22:417–431.
- Singer, S. J., and A. Kupfer. 1986. The directed migration of eukaryotic cells. *Annu. Rev. Cell Biol.* 2:337–365.
- Symons, M. H., and T. J. Mitchison. 1991. Control of actin polymerization in live and permeabilized fibroblasts. *J. Cell Biol.* 114:503–513.
- Trinkaus, J. P. 1984. Cells into organs. The Forces that Shape the Embryo. Prentice-Hall, Inc., Englewood Cliffs, NJ. 187–226.
- Wang, J. 1985. Exchange of actin subunits at the leading edge of living fibroblasts: possible role of treadmill. *J. Cell Biol.* 101:597–602.
- Wang, N., J. P. Butler, and D. E. Ingber. 1993. Mechanotransduction across the cell surface and through the cytoskeleton. *Science (Washington DC)* 260:1124–1127.
- Wagner, S. F. 1992. Introduction to Statistics. HarperCollins Publishers, Inc., New York. 195–213.
- Ward, M. D., and D. A. Hammer. 1993. A theoretical analysis for the effect of focal contact formation on cell-substrate attachment strength. *Biophys. J.* 64:936–959.